Accelerated Publications

Fluorescence Spectral Fluctuations of Single LH2 Complexes from *Rhodopseudomonas acidophila* Strain 10050†

Danielis Rutkauskas,*,‡ Vladimir Novoderezkhin,§ Richard J. Cogdell,|| and Rienk van Grondelle‡

Department of Biophysics and Physics of Complex Systems, Division of Physics and Astronomy, Faculty of Sciences, Vrije Universiteit, De Boelelaan 1081, 1081 HV Amsterdam, The Netherlands, A. N. Belozersky Institute of Physico-Chemical Biology, Moscow State University, Moscow 119899, Russia, and Division of Biochemistry and Molecular Biology, Institute of Biomedical and Life Sciences, University of Glasgow, Glasgow G12 8QQ, United Kingdom

Received February 2, 2004; Revised Manuscript Received February 26, 2004

ABSTRACT: We have investigated the energy landscape of the bacterial photosynthetic peripheral light-harvesting complex LH2 of purple bacterium *Rhodopseudomonas acidophila* by monitoring sequences of fluorescence spectra of single LH2 assemblies, at room temperature, with different excitation intensities as well as at elevated temperatures, utilizing a confocal microscope. The fluorescence peak wavelength of individual LH2 complexes was found to abruptly move between quasi-stable levels differing by up to 30 nm. These spectral shifts either to the blue or to the red were accompanied by a broadening and decrease of the intensity of the fluorescence spectrum. The frequency and size of these fluorescence peak movements were found to increase linearly with excitation intensity. Using the modified Redfield theory, changes in the realization of the static disorder accounted for the observed changes in spectral shape and intensity. Long lifetimes of the quasi-stable states suggest large free energy barriers between the different realizations.

Photosynthetic pigment−protein complexes play a decisive role in the collection of solar energy and the transfer of electronic excitation energy to the photosynthetic reaction center, where a charge separation is initiated (*1*, *2*). Since a high-resolution structure of the peripheral light-harvesting complex (LH2)[1] of the photosynthetic bacterium *Rhodopseudomonas acidophila* has become available (*3*, *4*), the molecule has played a key role in aiding our current understanding of photosynthetic light harvesting (*5*−*8*). LH2 of *Rps. acidophila* is a highly symmetric ring of nine protein−pigment subunits, each containing two helical transmembrane polypeptides, the α-polypeptide on the inner and the *β*-polypeptide on the outer side of the ring. The hydrophobic terminal of the protein binds a ring of 18 tightly coupled bacteriochlorophyll (BChl) molecules with a center−center distance of less than 1 nm between neighboring pigments. This ring is responsible for the intense absorption of LH2 at 850 nm (B850 ring). A second ring of nine weakly interacting BChls is located in the polar region of the protein and is largely responsible for the absorption around 800 nm (B800 ring).

From the detailed study of the spectroscopic and energy transfer properties of LH2, a consistent physical picture of the complex has emerged (*9*−*13*). All basic spectroscopic features can be understood on the basis of a model that includes both intrinsic disorder and excitonic coupling between the pigments (∼300 cm^{-1} for neighboring BChls in the B850 ring and ∼30 cm^{-1} for adjacent pigments in the B800 ring). Via introduction of relaxation between the elements of the so-called density matrix, the dynamics of vibrational and electronic coherence and excitation energy transfer have been described in great detail.

On the basis of room- and low-temperature single-molecule experiments, it has been proposed that the LH2 ring can deviate from the ideally circular structure (*14*−*17*). Room-temperature (RT) polarized fluorescence (FL) experiments were interpreted in terms of an elliptical absorber and emitter with ellipticity and directions of the principal axis varying as a result of the B800 and/or B850 distortion that destroys the rotational symmetry, traveling around the ring on a time scale of seconds (*17*). The anomalously large splitting of the two major orthogonal excitonic transitions observed in low-temperature polarized FL excitation spectra was attributed to a modulation of the coupling strength in the B850 ring that was asserted to be associated with an

† This research was supported by the Netherlands Organization for Scientific Research (NWO) (Project 809.38.001) and BBSRC.

* To whom correspondence should be addressed: Department of Biophysics and Physics of Complex Systems, Division of Physics and Astronomy, Faculty of Sciences, Vrije Universiteit, De Boelelaan 1081, 1081 HV Amsterdam, The Netherlands. Phone: +31 20 4447426. Fax: +31 20 4447999. E-mail: danielis@nat.vu.nl.

‡ Vrije Universiteit.

§ Moscow State University.

|| University of Glasgow.

[1] Abbreviations: FL, fluorescence; FLP, fluorescence peak; RT, room temperature; LH2, peripheral light-harvesting complex 2; BChl, bacteriochlorophyll; PR, participation ratio.

10.1021/bi0497648 CCC: $27.50
Published on Web 03/23/2004

elliptical deformation (*14*−*16*). Spectral diffusion of the B800 band of LH2, observed in the low-temperature experiments, was also attributed to structural alterations (*18*). These spectral fluctuations of different magnitudes occurring on different time scales were associated with the hierarchical structure of the protein conformational landscape (*19*). Smaller ellipticities of 0.95−0.91 were found in AFM measurements of loosely packed LH2s in membrane, and were probably partly due to an interplay of the disrupting tip and stabilizing lipid environment effects (*20*). On the other hand, isolated LH2s in the scaffold of detergent molecules clearly deviated from a ringlike shape (*21*). In general, the observed variation of the spectral and functional properties of LH2 suggests that the complex can undergo a variety of deformations. It is reasonable to assume that such dynamic structural alterations also underlie the pattern of the static disorder of pigment site energies that play a key role in understanding the spectroscopic and energy transfer properties of LH2.

In the work presented here, we investigate these dynamic fluctuations under physiological conditions, as manifested by the time evolution of the FL spectrum. To do so, we have acquired series of FL spectra of single LH2 complexes at room temperature and elevated temperatures with various excitation intensities.

MATERIALS AND METHODS

Sample Preparation and Immobilization. Isolated LH2 complexes were immobilized on a standard microscope coverslip treated with a 0.01% poly-L-lysine (PLL, Sigma) solution. The coverslip was used as a base for a home-designed, hermetic, temperature-controlled sample cell.

Purified LH2 complexes of *Rps. acidophila* were prepared as described previously (*22*, *23*). The sample stock solution of 0.62 μM LH2 in buffer [20 mM Tris-HCl (pH 8.0) and 0.1% lauryldimethylamine oxide (LDAO)] was kept at −80 °C prior to being thawed. It was diluted in the same buffer in two steps by a factor of 2×10^4. A 20 μL drop of a 33 pM LH2 solution was placed on the coverslip, and the sample cell was assembled. After a few minutes, the cell volume was washed with deoxygenated, 0.1% LDAO-containing buffer, thus removing the access sample and submerging the immobilized single molecules in an oxygen-free environment. Oxygen was thoroughly removed from the buffer by flowing gaseous nitrogen and by agitating the buffer with a magnetic spinner to a level that cannot be detected with an electrolytic oxygen meter.

Experimental Setup. FL images and spectra were acquired with a confocal microscope based on a commercial inverted microscope (Nikon, Eclipse TE300). The excitation source was a Ti:sapphire laser system (Coherent, Mira 900) producing 3 ps, 800 nm pulses with a repetition rate of 76 MHz. A dichroic beam splitter (Chroma Technology Corp., 815dclp) reflected the laser beam into the objective lens (Nikon, Plan Fluor 100×, 1.3 NA, oil immersion), focusing the excitation light onto the glass−water interface in the sample cell to a diffraction-limited spot (fwhm of ∼600 nm). The intensities used in the experiments (from 0.13 to 1.6 kW/cm^2 or equivalently 500 nW to 6 μW) represent the values at this interface. The emission was filtered with a 100 μm pinhole and single 130 nm interference filter (Chroma Technology Corp., HQ885/130m).

The sample cell was mounted on a closed loop two-dimensional piezo stage (Physik Instrumente, P-731.8C) controlled by a digital four-channel controller (Physik Instrumente, E-710.4LC).

To obtain images, emission was detected with a Si avalanche photodiode single photon-counting module (SPCM-AQR-16, Perkin-Elmer Optoelectronics) and counter timer board (National Instruments, PCI-6602). Spectra were acquired by dispersing the fluorescence onto a liquid nitrogen-cooled back-illuminated charge-coupled device (CCD) camera chip (Princeton Instruments, Roper Scientific, Spec10: 100BR). CCD pixels were binned along the spectroscopic axis to yield a resolution of <1 nm. Fluorescence detection in both image and spectral acquisition modes was indiscriminate of signal polarization. The polarization sensitivity of the detection due to the dispersing element was not explicitly taken into account. However, because of a wide angle of acceptance of the high-numerical aperture objective, we expect the effect of polarization sensitivity to be small.

Images and Spectra. A FL image is acquired by continuously sweeping the piezo stage over the laser focus with a frequency of 3 Hz while its position in the perpendicular direction is changed by 100 nm for each line; the FL signal is concomitantly detected with an APD. Images are then constructed by associating the piezo stage coordinate with the corresponding intensity. The scanning covers a 10 μm × 10 μm area. After the coordinates of bright particles are determined, the piezo stage is positioned to bring the particle into the focus of the objective, and after the mode is switched to a spectroscopic one, a series of FL spectra is collected for 2 min with an integration time (0.5−2 s) that is dependent on the excitation power and the sample temperature. At higher excitation intensities and lower temperatures, shorter integration times are sufficient for the collection of the spectra with a satisfactory signal-to-noise ratio. The excitation intensity and the ambient conditions remain unchanged during the acquisition.

Data Analysis. For a quantitative analysis, the acquired spectra are fitted with a skewed Gaussian function, using a nonlinear Levenberg−Marquardt fitting method. The expression for the skewed Gaussian function is

$$F(\lambda) = \Delta + A \exp\{-\ln(2)/b^2 \ln[1 + 2b(\lambda - \lambda_m)/\Delta\lambda]\}^2$$

where Δ is the offset, A the amplitude, λ_m the fluorescence peak (FLP) wavelength, $\Delta\lambda$ the width, and b the skewness.

The fwhm of the spectrum is calculated from the width and the skewness. Consequently, by fitting each spectrum from a series, we obtain the time traces of the amplitude, the fwhm, and the FLP with the corresponding confidence margins.

RESULTS

The primary objective of this study was to investigate if we could observe fluctuations of peak position, width, and intensity of emission spectrum of single LH2 complexes as a measure of structural dynamics, which can occur in this complex. This was achieved by collecting series of single-molecule FL spectra at RT and variable excitation intensity as well as at elevated temperatures. In total, close to 1000 molecules were studied under various ambient conditions. Intrinsic (i.e., measured with a low excitation power)

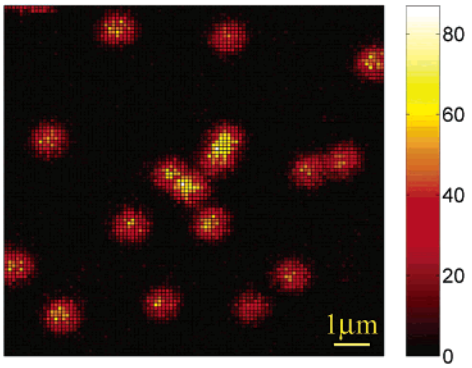

FIGURE 1: FL image of single LH2 complexes.

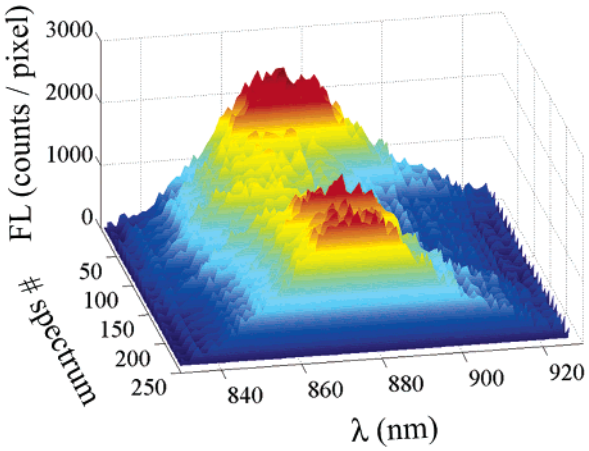

FIGURE 2: Series of FL spectra of single LH2.

fluctuations proved to be insignificant on the time scale of our experiment (2 min). However, increasing the excitation power introduced prominent spectral jumps and changes in the spectral shape and intensity of the emission. To a smaller extent, the same effect could be detected in experiments at elevated temperatures (28 and 35 °C), though the stability of the LH2 complexes was decreased significantly.

Earlier experiments (*17*) have shown that the survival time of the illuminated LH2 complexes strongly depends on the presence of oxygen in the environment. We observed that irreversible photobleaching of an oxygen-containing sample took place over the course of seconds or tens of seconds, and even when kept in the dark, the oxygen-containing preparation degraded in a few hours at RT. On the other hand, careful removal of oxygen from the ambient sample prolonged the bright state of single LH2s to minutes or even tens of minutes in some cases, and the sample remained suitable for measurements for 2 days. For the reasons given above, all the single-molecule measurements presented in this work were carried out on oxygen-free samples.

Images. An example of a raw FL image of LH2 assemblies immobilized on a PLL-treated coverslip is shown in Figure 1. Each image is 100 pixels × 100 pixels (0.1 μm per pixel). The pixel integration time is 3 ms. The excitation intensity at 800 nm is 3.5 μW. The background is $\leq$10 counts/pixel, and the maximum intensity is 87 counts/pixel. Although particles appear to be similar in integral intensity, in reality they are distributed over a range of 1300−2500 counts, which is probably partly due to the polarization effects of the excitation absorption and emission (since single complexes are immobilized on an atomically nonflat glass surface) and partly to the tendency of the emission intensity to fluctuate. We also do not exclude the possibility of observing aggregated complexes or adjacent complexes appearing as one particle. To make sure that we monitor only single LH2s, excessively bright particles are discarded and spectral measurements are carried out on molecules constituting the bulk of the intensity distribution.

FL Spectra. A typical series of FL spectra of a single LH2 enabling the observation of the spectral diffusion is presented in Figure 2. It results from a sequence of 240 single LH2 spectra via summation of each 10 consecutive spectra for clarity. The spectrum integration time is 0.5 s, and the excitation intensity at 800 nm is 6 μW. In this experiment, the FL amplitude and the FLP diffuse dramatically. Spectra at the beginning of the series have a relatively high amplitude and an intermediate FLP, whereas in the course of the measurement, the amplitude subsides with the FLP shifting to the blue; both parameters recover at the end of the series. Notably, the width of a single complex FL spectrum is comparable with that of the bulk spectrum (data not shown).

FLP Traces. FLP time traces of four individual particles are shown in Figure 3. The spectrum integration time is 0.5 s, and the excitation intensity at 800 nm is 6 μW. Though acquired with the same excitation intensity and ambient conditions, the traces are qualitatively different. The FLP fluctuates weakly in Figure 3A, while panels B and C of Figure 3 demonstrate notable spectral jumps to the blue and to the red relative to the initial FLP value, respectively. Interestingly, the FLP abruptly jumps between the various levels of almost constant magnitude, and even more remarkably, it regains a value close to the initial one before the end of the trace. Unexpectedly, the complex spends a number of seconds in each of the stable states before it moves to a different state. Figure 3D shows spectral diffusion in both directions. The spectrum of a single particle first drifts to longer wavelengths, then abruptly jumps to the blue, and finally settles at a FLP that is shifted to the blue by ~15 nm relative to the initial FLP, preventing the unambiguous classification of this particle as one that performs a spectral jump in one direction. We note that these conspicuous spectral jumps are in many cases reversible, and the initial FLP value (or a value close to it) is regained (Figure 3B,C). For other particles, the initial FLP is not recovered before photobleaching occurs (Figure 3D) (or rather an apparent photobleaching; we have observed the recovery of the emission of some complexes after dark periods of more than 2 min, data not shown). From Figure 3C, it appears that the LH2 bleaching does not occur as a single event; after the complex enters a dark state for a few seconds, its emission reappears with a different FLP position. On the other hand, the spectral diffusion can occur without the temporary loss of the radiative power, as shown in the Figure 3B. From all the particles measured with the excitation intensities in the range from 1.5 to 6 μW, ~10% exhibited the steplike character of the FLP position traces.

Light-Induced Spectral Fluctuations. In this work, we confine ourselves to a qualitative description of the spectral properties of the strongly fluctuating particles. A detailed account of the relevant statistics will be presented elsewhere (D. Rutkauskas *et al*., manuscript in preparation). In summary, we observed that few spectral jumps of the single LH2 occur at low excitation intensity and RT, but the frequency

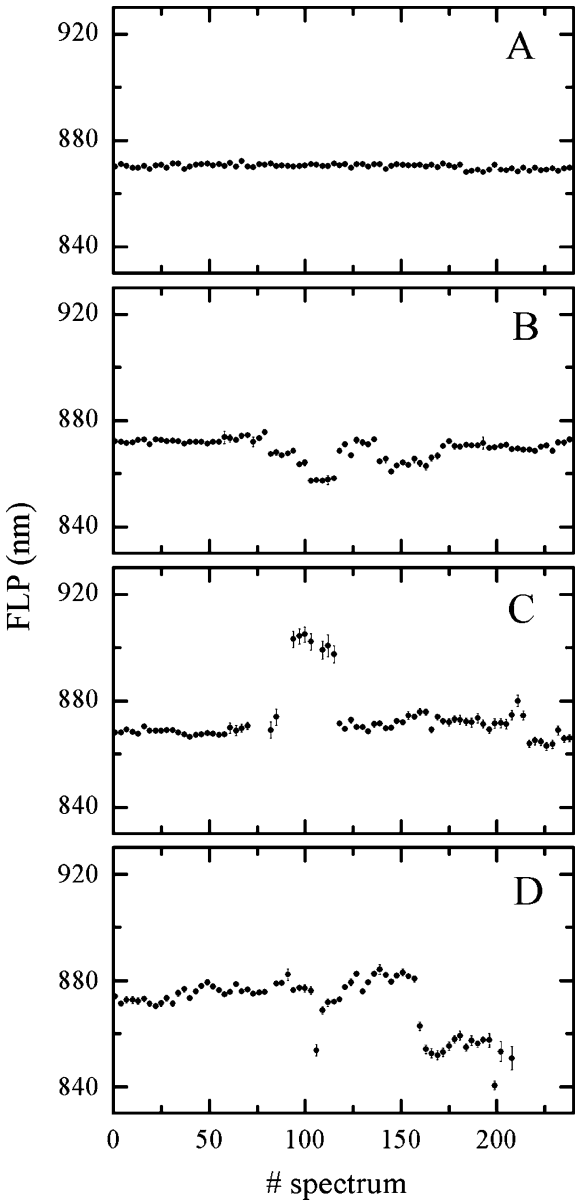

FIGURE 3: FLP time traces of four individual LH2s. Various spectral diffusion scenarios: (A) relatively constant FLP, (B) spectral jumps to the blue, (C) spectral jump to the red, and (D) spectral jumps to both the red and blue. Only every third data point is presented for clarity.

of their occurrence increases with an increase in excitation intensity and to a much lesser extent with temperature elevation. Thus, spectral diffusion in our experiment is mostly light induced. However, since the observed spectral jumps are reversible (Figure 3), we conclude that even with the highest excitation intensity used here, the LH2 complex is not driven into conformational states from which it can no longer escape. Instead, stronger excitation or an elevated temperature enables an exploration of a broader range of states in a finite span of the experimental time.

Some of the strongly fluctuating LH2 assemblies exhibited a strong correlation between the temporal changes of the FLP and the amplitude and/or between the FLP and the fwhm. We observed that these correlations might be either positive or negative; for example, some single LH2s display a negative jump of the FLP (blue shift) with a concomitant increase of the fwhm (negative correlation), and others undergo an increase in FLP (red shift) that is connected with an increment of the fwhm (positive correlation). Overall, we observe that if a particle undergoes significant spectral diffusion, accompanied by the correlated evolution of two or all three spectral fit parameters, then an FLP increase or reduction is associated with a spectral broadening and a decrease of radiative power.

In summary, the main observations made in our experiment are that abrupt light-induced jumps of FLP occur between levels distinctly different in magnitude, a complex dwells for a relatively long time in one of the quasi-stable states, and FLP jumps are accompanied by spectral broadening and a decrease in amplitude.

DISCUSSION

Excitation Dynamics. After the B800 ring in the LH2 complex absorbs a photon, energy is transferred to the B850 BChl molecules in ~1 ps (*24*, *25*) with a very high efficiency since the competing processes of FL and nonradiative decay are 3 orders of magnitude slower (*26*). Subsequently, exciton relaxation and excitation hopping will occur in the B850 ring, with a certain probability leading to FL.

When one considers that the molar absorption coefficient of LH2 at 800 nm is 2.3×10^6 M^{-1} cm^{-1} (*10*), a single complex will absorb 8.6×10^6 photons/s, if positioned in the center of the Gaussian laser beam, delivering 1 μW of CW excitation at 800 nm. The Bchl triplet with a lifetime of 70 μs (*27*) is formed with a 2−15% yield (*27*, *28*) and is efficiently transferred to the carotenoid which has a triplet lifetime of ~10 μs (*29*). This triplet is a very efficient trap of the singlet Bchl excitations due to S−T annihilation. In the triplet-free state, the FL quantum efficiency is 10% (*26*). From the simple calculation with the above parameters, it follows that in the presence of the carotenoid triplet, the FL yield decreases by a factor of 200. The frequency of triplet formation is dependent on the triplet yield and excitation intensity. Thus, the resulting fluorescence yield considering the presence of the triplet is dependent on the same parameters. The observed average FL count rate is ~8500 counts/s at an excitation intensity of 500 nW. With the estimated signal collection efficiency of 8%, we would expect to achieve this level of signal with a 9% (in the middle of the range of values; see above) triplet formation yield which corresponds to the resulting FL quantum efficiency of 2.5%.

This analysis implies that only a fraction of the absorbed excitation photons is re-emitted as FL. The remaining excitations either decay radiationlessly directly to the ground state, form a triplet, or are quenched by triplets. In either case, the absorbed excitation energy is eventually dissipated as heat, which leads to a temperature increase of the pigment surroundings. However, despite the large number of excitations produced in the system, we only seldom observe spectral changes. The complex appears to dwell for a relatively long time in one of the quasi-stable states, characterized by a specific peak position, shape, and intensity of emission. We thus conclude that the free energy barriers separating those quasi-stable states must be large.

Local temperature increase is a plausible cause of the structural alterations that we will associate with a change in the realization of the static disorder of the electronic transition energies in the system that is in turn connected to particular

spectral properties. Below, we develop a model that accounts for the observed changes in the spectral profile and position as a result of the spectral jumping.

A Quantitative Description of Single-Molecule Emission Spectra. In our model of the B850 ring, we utilize the modified Redfield approach that incorporates excitonic interactions, static disorder of the electronic transition energies of the pigments, and strong coupling of the electronic transitions to nuclear motions (phonons). The coupling to the fast nuclear motions determines the optical line shape in both conventional (*30*) and single-molecule spectroscopy (*31*). Slow nuclear motions result in different equilibrium positions of the nuclear coordinates, i.e., are associated with the evolution of the pigment−protein conformations on a microsecond to second time scale, and produce different realizations of the static disorder of the electronic transition energies (*32*). They are the cause of the inhomogeneous broadening of the bulk spectrum. Particular nuclear coordinates result in states of a single complex, characterized by a certain FLP and a line shape. Thermally activated slow nuclear motions lead to the transitions between these states, observed as abrupt jumps in the FLP traces (Figure 3). Here we will not consider the dynamics of such transitions, but restrict ourselves to the modeling of the FL line shapes for different realizations of the disorder.

The energies of the exciton levels are calculated by constructing and diagonalizing the one-exciton Hamiltonian. B850 BChls in the dimeric subunit of LH2 are assumed to have unperturbed transition energies of 12 415 and 12 215 cm^{-1} that were adjusted from a fit of a bulk spectrum. The nearest neighbor interaction energies inside the protein dimer and between pigments of adjacent dimers were taken to be 291 and 273 cm^{-1}, respectively (*9*). The static disorder of the transition energies was taken into account by introducing uncorrelated variations randomly taken from a Gaussian distribution with a fwhm of σ. The numerical diagonalization of the Hamiltonian (for each realization of the disorder) gives the energies of the exciton states, ω_k, and the wave function amplitudes, c_n^k, (participation of the nth pigment site in the kth exciton state).

The absorption and FL line shapes of the exciton states are calculated assuming strong exciton−phonon coupling (*33*). The homogeneous absorption line shape for the kth exciton state is expressed in terms of the line broadening function, g_k. The steady state Stokes shift of the emission maximum of the kth state is given by $2\lambda_k$, where λ_k is the reorganization energy. Both g_k and λ_k are related to the spectral density, $C_k(\omega)$, in the exciton basis, which is connected with the spectral density in the site representation, $C_n(\omega)$, through the fourth power of the wave function amplitudes; i.e., $C_k(\omega) = \sum_n (c_n^k)^4 C_n(\omega)$. Here we have assumed that the phonon-induced modulation of the electronic transition is described by an uncorrelated diagonal disorder (not to be confused with static disorder). The $\sum_n (c_n^k)^4$ factor is also known as the participation ratio (PR), or inverse delocalization length of the kth exciton state. Thus, the phonon-induced broadening and the Stokes shift of the exciton level are dependent on the PR of that level.

The spectral density $C_n(\omega)$ is assumed to have the form of an overdamped Brownian oscillator (*30*, *33*) with a coupling parameter λ and a relaxation time τ. In our model, λ and τ (as well as σ) are site-independent free parameters adjusted from the fit of the bulk absorption and FL spectra.

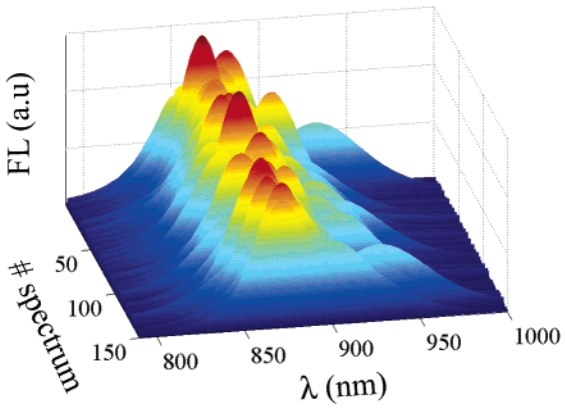

FIGURE 4: FL profiles calculated for 150 realizations of the disorder for a single LH2 complex at RT.

The model also regards the relaxation-induced broadening; i.e., we suppose an additional homogeneous broadening of the exciton states given by their inverse lifetimes; $R_k = -\sum_{k'} R_{k'k'kk}$, where $R_{k'k'kk}$ is the rate of the $k \rightarrow k'$ transition calculated (*33*) in terms of g_k functions.

The RT bulk absorption and FL spectra of the B850 ring can be reproduced with the following parameter values: $\sigma = 370$ cm^{-1}, $\lambda = 220$ cm^{-1}, and $\tau = 70$ fs. Introducing higher static and dynamic disorder values, i.e., $\sigma = 450$ cm^{-1} and $\lambda = 370$ cm^{-1}, improved even further a fit of the single-molecule FL spectra profiles.

Single LH2 FL profiles calculated for 150 realizations of the static disorder at RT are shown in Figure 4. The FLP positions are distributed over a range of values similar to the experimental data. However, since we do not have an explicit model to describe the dynamics of spectral jumping, the collection of calculated FLPs (Figure 4) does not represent temporal evolution of the spectrum.

Figure 5A−C contains three experimental profiles that are averages of all single-molecule FL spectra measured with an excitation intensity of 3.5 μW and peaking in intervals of 859−861, 869−871, and 889−891 nm. These average spectra have fwhm values of 53, 48, and 67 nm, respectively. The red-shifted spectrum (Figure 5C) is significantly broadened and has a pronounced short-wavelength wing. Spectra with the blue-shifted and intermediate FLP positions (panels A and B of Figure 5, respectively) feature a regular FL profile asymmetry, i.e., a broader long-wavelength tail. Notably, the blue- and red-shifted spectra are broader than that with an intermediate FLP position. For comparison, a number of calculated FL profiles corresponding to different realizations of the static disorder have been collected into three groups with their peak positions belonging to narrow intervals of 859−862, 871−873, and 886−892 nm around the corresponding experimentally determined values. The average calculated FL profile has a maximum near 870 nm. Realizations with the FLP near this wavelength occur with the highest probability. Overlaying of experimental and simulated curves in Figure 5A−C shows that the model satisfactorily reproduces all the features of the experimental spectra.

The FL line shapes and their peak positions are determined by a specific realization of the static disorder, which is related to a particular excitonic energy level structure. Typical patterns of such structure corresponding to the three experi-

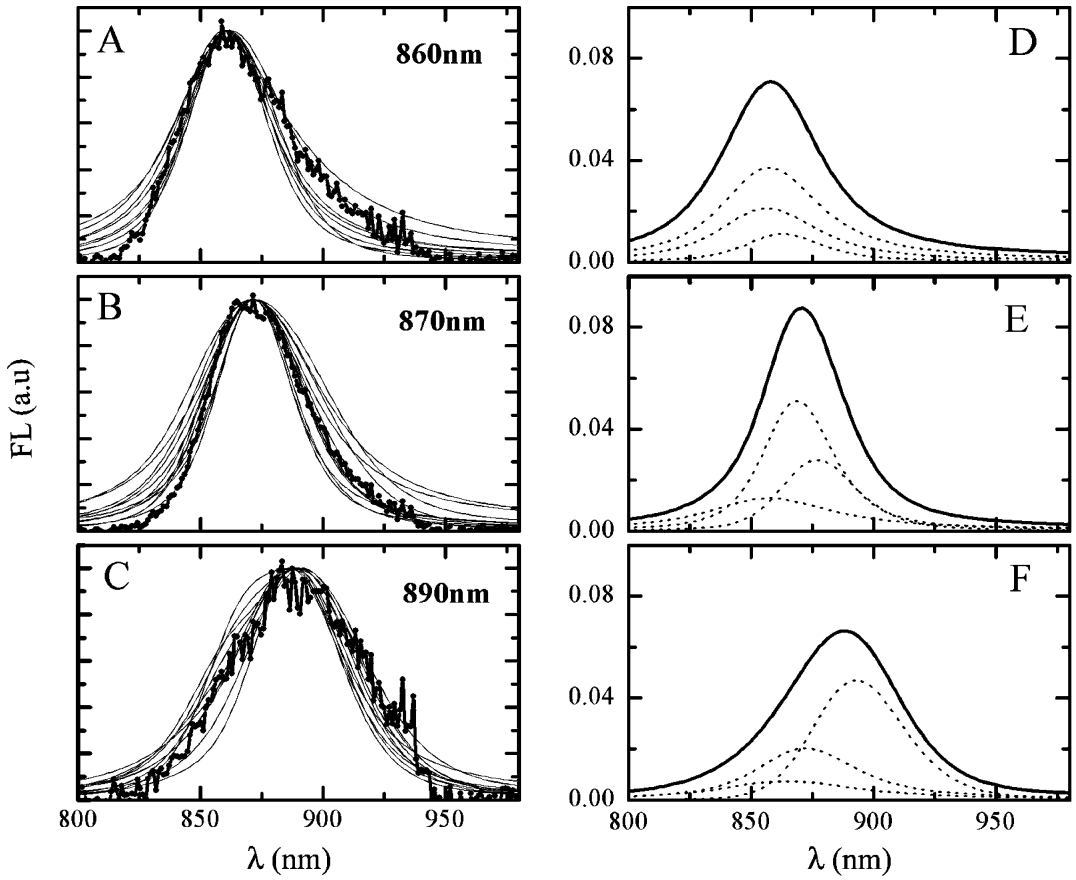

FIGURE 5: Experimental (points connected with the thick solid line) and calculated (solid thin line) FL profiles: (A) blue-shifted, (B) intermediate, and (C) red-shifted. (D−F) Three typical realizations of disorder resulting in FL profiles with different FLP positions, shown together with contributions from the three lowest exciton states (dashed lines). The spectra are not normalized for the comparison of their relative amplitudes (parameters of these three realizations are also given in Table 1).

Table 1: Positions of FLP and FL Amplitudes of the Three FL Profiles Shown in Panels D−F of Figure 5, Together with the Corresponding PRs for the Lowest Exciton Components ($k = 0, -1$, and 1)

	FLP of 859 nm	FLP of 871 nm	FLP of 888 nm
FL amplitude (arbitrary units)	0.077	0.094	0.070
$k = 0$	0.107	0.203	0.356
$k = -1$	0.098	0.139	0.157
$k = 1$	0.131	0.087	0.180

mentally measured FLP positions at 859, 871, and 888 nm (Figure 5A−C) are shown in panels D−F of Figure 5, respectively. The corresponding PRs of the exciton levels, shown in Figure 5D−F, are listed in Table 1. For a circular aggregate of N molecules, the PR = $1/N$ for the lowest and $3/(2N)$ for the higher states in the absence of the disorder. In the case of the LH2 ring, $N = 18$ and the PR is calculated to be 0.056 and 0.083, respectively. Including the disorder results in a dramatic increase of the lowest state PR. For LH2 with a realistic value for the disorder, the PR = 0.1−0.15 for the higher states and 0.15−0.35 for the lowest state, with an increasing PR value for the red-shifted levels (*10*, *34*−*36*). The phonon-induced broadening is related to a certain PR value; thus, the red-shifted excitonic levels are additionally broadened by an enhanced phonon coupling.

Table 1 and Figure 5D show that the blue-shifted FL profile corresponds to a relatively delocalized state. Indeed, the PRs for all three excitonic levels are relatively small and consequently must be associated with small contributions from specific sites, thus implying that the excitation is delocalized over different sites. Consequently, an excitonic structure of these levels is not destroyed by the disorder. The lowest state is only weakly allowed (the corresponding band has a small amplitude) so that the RT emission originates mostly from the degenerate $k = \pm 1$ pair, giving rise to a blue-shifted FL.

Realization of a larger static disorder (Figure 5E and the second row in Table 1) results in a larger splitting between the $k = \pm 1$ levels so that the lower $k = -1$ state becomes more populated and more emissive as compared to the $k = 1$ state. However, both $k = -1$ and $k = 1$ levels still remain delocalized (PR = 0.087−0.139). The lowest $k = 0$ state becomes more localized (PR = 0.2), more radiant, and more red-shifted. Such an exciton structure is characteristic of the realizations with the FLP near the maximum of the bulk emission spectrum.

Figure 5F shows an example of a red-shifted FL profile. The exciton structure is strongly affected by the disorder, which induces a large splitting between the three lowest states. The PR value is relatively large for all the states and especially for the lowest one. Because of the large splitting between the exciton levels, the FL originates mostly from the lowest state. Its localized character (PR $\geq$ 0.35) gives rise to an increased phonon coupling, which leads to a significant broadening of the $k = 0$ level. Because of a larger Stokes shift, the emission is also further red shifted.

Downhill exciton relaxation with a rate increasing for the higher levels is an additional line-broadening factor contributing to the width of the blue-shifted FL spectrum. In our model, $R_k = 16$, 29, 44, and 57 ps^{-1} for the $k = 0$, -1, 1, and -2 levels, respectively. The more pronounced relaxation broadening of the $k = \pm 1$ levels results in a larger width of the blue-shifted FL spectra (determined mostly by the $k = \pm 1$ emission). If the relaxational broadening is disregarded, a blue shift would always be accompanied by the narrowing of the FL line. Indeed, the $k = \pm 1$ levels are narrower than the $k = 0$ levels, since the corresponding PR values, and consequently the phonon couplings, are smaller.

Calculated amplitudes of FL corresponding to the three typical realizations of disorder (Table 1) reproduce the experimentally observed decrease in spectral amplitude upon spectral jumping.

In summary, we have experimentally observed notable light-induced jumps in the FLP position between the levels of distinctly different magnitude. Though spectral fluctuations were evidently light-induced, they did not signal the deterioration of the assembly, since jumps were reversible. We conclude that the excitation intensity drives the complex into conformational states, which are less accessible under dark conditions, but still intrinsic to the system.

The observed spectral jumps were accompanied by a broadening of the FL profile and a decrease in amplitude. We have qualitatively accounted for these effects by modeling the FL with different realizations of the static disorder of pigment transition energies. However, our model does not encompass the dynamics of the spectral jumps. The observation that large spectral jumps occur with a very low probability with respect to the number of excitations received by the system leads us to conclude that large free energy barriers separate the states with distinctly different spectral properties.

ACKNOWLEDGMENT

We thank Ph.D. M. Papagianakis, Ph.D. S. Georgakopoulou, and Ph.D. D. Larsen for critically reading the manuscript and Ph.D. M. Vengris and Ph.D. E. Peterman for fruitful discussions in building the experimental setup.

REFERENCES

1. van Grondelle, R. (1985) Excitation energy transfer, trapping and annihilation in photosynthetic systems, *Biochim. Biophys. Acta 811*, 147−195.
2. van Grondelle, R., Dekker, J. P., Gillbro, T., and Sundström, V. (1994) Energy Transfer and Trapping in Photosynthesis, *Biochim. Biophys. Acta 1187*, 1−65.
3. McDermott, G., Prince, S. M., Freer, A. A., Hawthornthwaitelawless, A. M., Papiz, M. Z., Cogdell, R. J., and Isaacs, N. W. (1995) Crystal Structure of an Integral Membrane Light-Harvesting Complex from Photosynthetic Bacteria, *Nature 374*, 517−521.
4. Papiz, M. Z., Prince, S. M., Howard, T., Cogdell, R. J., and Isaacs, N. W. (2003) The structure and thermal motion of the B800−850 LH2 complex from *Rps. acidophila* at 2.0 Å resolution and 100 K: New structural features and functionally relevant motions, *J. Mol. Biol. 326*, 1523−1538.
5. Cogdell, R. J., Fyfe, P. K., Barrett, S. J., Prince, S. M., Freer, A. A., Isaacs, N. W., McGlynn, P., and Hunter, C. N. (1996) The purple bacterial photosynthetic unit, *Photosynth. Res. 48*, 55−63.
6. Sundström, V., Pullerits, T., and van Grondelle, R. (1999) Photosynthetic light-harvesting: Reconciling dynamics and structure of purple bacterial LH2 reveals function of photosynthetic unit, *J. Phys. Chem. B 103*, 2327−2346.
7. Hu, X. C., Ritz, T., Damjanovic, A., Autenrieth, F., and Schulten, K. (2002) Photosynthetic apparatus of purple bacteria, *Q. Rev. Biophys. 35*, 1−62.
8. Robert, B., Cogdell, R. J., and van Grondelle, R. (2003) *Light-harvesting antennas in photosynthesis*, Vol. 13, Kluwer Academic Publishers, Dordrecht, The Netherlands.
9. Sauer, K., Cogdell, R. J., Prince, S. M., Freer, A., Isaacs, N. W., and Scheer, H. (1996) Structure-based calculations of the optical spectra of the LH2 bacteriochlorophyll-protein complex from *Rhodopseudomonas acidophila*, *Photochem. Photobiol. 64*, 564−576.
10. Alden, R. G., Johnson, E., Nagarajan, V., Parson, W. W., Law, C. J., and Cogdell, R. J. (1997) Calculations of spectroscopic properties of the LH2 bacteriochlorophyll-protein antenna complex from *Rhodopseudomonas acidophila*, *J. Phys. Chem. B 101*, 4667−4680.
11. Hu, X. C., Ritz, T., Damjanovic, A., and Schulten, K. (1997) Pigment organization and transfer of electronic excitation in the photosynthetic unit of purple bacteria, *J. Phys. Chem. B 101*, 3854−3871.
12. Wu, H. M., Rätsep, M., Lee, I. J., Cogdell, R. J., and Small, G. J. (1997) Exciton level structure and energy disorder of the B850 ring and the LH2 antennal complex, *J. Phys. Chem. B 101*, 7654−7663.
13. Scholes, G. D., and Fleming, G. R. (2000) On the mechanism of light harvesting in photosynthetic purple bacteria: B800 to B850 energy transfer, *J. Phys. Chem. B 104*, 1854−1868.
14. van Oijen, A. M., Ketelaars, M., Köhler, J., Aartsma, T. J., and Schmidt, J. (1999) Unraveling the electronic structure of individual photosynthetic pigment−protein complexes, *Science 285*, 400−402.
15. Matsushita, M., Ketelaars, M., van Oijen, A. M., Köhler, J., Aartsma, T. J., and Schmidt, J. (2001) Spectroscopy on the B850 band of individual light-harvesting 2 complexes of *Rhodopseudomonas acidophila* II. Exciton states of an elliptically deformed ring aggregate, *Biophys. J. 80*, 1604−1614.
16. Ketelaars, M., van Oijen, A. M., Matsushita, M., Köhler, J., Schmidt, J., and Aartsma, T. J. (2001) Spectroscopy on the B850 band of individual light-harvesting 2 complexes of *Rhodopseudomonas acidophila* I. Experiments and Monte Carlo simulations, *Biophys. J. 80*, 1591−1603.
17. Bopp, M. A., Sytnik, A., Howard, T. D., Cogdell, R. J., and Hochstrasser, R. M. (1999) The dynamics of structural deformations of immobilized single light-harvesting complexes, *Proc. Natl. Acad. Sci. U.S.A. 96*, 11271−11276.
18. van Oijen, A. M., Ketelaars, M., Köhler, J., Aartsma, T. J., and Schmidt, J. (2000) Spectroscopy of individual light-harvesting 2 complexes of *Rhodopseudomonas acidophila*: diagonal disorder, intercomplex heterogeneity, spectral diffusion, and energy transfer in the B800 band, *Biophys. J. 78*, 1570−1577.
19. Hofmann, C., Aartsma, T. J., Michel, H., and Kohler, J. (2003) Direct observation of tiers in the energy landscape of a chromoprotein: A single-molecule study, *Proc. Natl. Acad. Sci. U.S.A. 100*, 15534−15538.
20. Scheuring, S., Reiss-Husson, F., Engel, A., Rigaud, J. L., and Ranck, J. L. (2001) High-resolution AFM topographs of *Rubrivivax gelatinosus* light-harvesting complex LH2, *EMBO J. 20*, 3029−3035.
21. Hong, X., Weng, Y.-X., and Li, M. (2004) Determination of the Topological Shape of Integral Membrane Protein Light-Harvesting Complex LH2 from Photosynthetic Bacteria in the Detergent Solution by Small-Angle X-ray Scattering, *Biophys. J. 86*, 1082−1088.
22. Halloren, E., McDermott, G., Lindsay, J. G., Miller, C., Freer, A. A., Isaacs, N. W., and Cogdell, R. J. (1995) Studies on the Light-Harvesting Complexes from the Thermotolerant Purple Bacterium *Rhodopseudomonas cryptolactis*, *Photosynth. Res. 44*, 149−155.
23. Cogdell, R. J., and Hawthornthwaite, A. M. (1993) *Preparation, purification and crystallization of purple bacterial antenna complexes*, Vol. 1, Academic Press, New York.
24. Ma, Y. Z., Cogdell, R. J., and Gillbro, T. (1997) Energy transfer and exciton annihilation in the B800−850 antenna complex of the photosynthetic purple bacterium *Rhodopseudomonas acidophila* (Strain 10050). A femtosecond transient absorption study, *J. Phys. Chem. B 101*, 1087−1095.
25. Salverda, J. M., van Mourik, F., van der Zwan, G., and van Grondelle, R. (2000) Energy transfer in the B800 rings of the peripheral bacterial light-harvesting complexes of *Rhodopseudo-*

monas acidophila and *Rhodospirillum molischianum* studied with photon echo techniques, *J. Phys. Chem. B 104*, 11395−11408.
26. Monshouwer, R., Abrahamsson, M., van Mourik, F., and van Grondelle, R. (1997) Superradiance and exciton delocalization in bacterial photosynthetic light-harvesting systems, *J. Phys. Chem. B 101*, 7241−7248.
27. Monger, T. G., Cogdell, R. J., and Parson, W. W. (1976) Triplet States of Bacteriochlorophyll and Carotenoids in Chromatophores of Photosynthetic Bacteria, *Biochim. Biophys. Acta 449*, 136−153.
28. Cogdell, R. J., Hipkins, M. F., MacDonald, W., and Truscott, T. G. (1981) Energy transfer between the carotenoid and the bacteriochlorophyll within the B-800−850 light-harvesting pigment−protein complex of *Rhodopseudomonas sphaeroides*, *Biochim. Biophys. Acta 634*, 191−202.
29. Angerhofer, A., Bornhauser, F., Gall, A., and Cogdell, R. J. (1995) Optical and Optically Detected Magnetic-Resonance Investigation on Purple Photosynthetic Bacterial Antenna Complexes, *Chem. Phys. 194*, 259−274.
30. Mukamel, S. (1995) *Principles of Nonlinear Optical Spectroscopy*, Oxford University Press, New York.
31. Jung, Y., Barkai, E., and Silbey, R. J. (2002) Current status of single-molecule spectroscopy: Theoretical aspects, *J. Chem. Phys. 117*, 10980−10995.
32. Dempster, S. E., Jang, S. J., and Silbey, R. J. (2001) Single molecule spectroscopy of disordered circular aggregates: A perturbation analysis, *J. Chem. Phys. 114*, 10015−10023.
33. Zhang, W. M., Meier, T., Chernyak, V., and Mukamel, S. (1998) Exciton-migration and three-pulse femtosecond optical spectroscopies of photosynthetic antenna complexes, *J. Chem. Phys. 108*, 7763−7774.
34. Novoderezhkin, V., Monshouwer, R., and van Grondelle, R. (1999) Disordered exciton model for the core light-harvesting antenna of *Rhodopseudomonas viridis*, *Biophys. J. 77*, 666−681.
35. Novoderezhkin, V., Monshouwer, R., and van Grondelle, R. (1999) Exciton (de)localization in the LH2 antenna of *Rhodobacter sphaeroides* as revealed by relative difference absorption measurements of the LH2 antenna and the B820 subunit, *J. Phys. Chem. B 103*, 10540−10548.
36. Novoderezhkin, V., Wendling, M., and van Grondelle, R. (2003) Intra- and interband transfers in the B800−B850 antenna of *Rhodospirillum molischianum*: Redfield theory modeling of polarized pump−probe kinetics, *J. Phys. Chem. B 107*, 11534−11548.

BI0497648